Aeolian transport and deposition of plant wax *n*-alkanes across the tropical North Atlantic Ocean

Laura T. Schreuder [a], Jan-Berend W. Stuut [b,c], Laura F. Korte [b], Jaap S. Sinninghe Damsté [a,d], Stefan Schouten [a,d,∗]

[a] NIOZ Royal Netherlands Institute for Sea Research, Department of Marine Microbiology and Biogeochemistry, and Utrecht University, P.O. Box 59, 1790 AB Den Burg, Texel, The Netherlands
[b] NIOZ Royal Netherlands Institute for Sea Research, Department of Ocean Systems, and Utrecht University, P.O. Box 59, 1790 AB Den Burg, Texel, The Netherlands
[c] MARUM, Center for Marine Environmental Sciences, University of Bremen, Bremen, Germany
[d] Department of Earth Sciences, Faculty of Geosciences, Utrecht University, P.O. Box 80.121, 3508 TA Utrecht, The Netherlands

ABSTRACT

Long chain *n*-alkanes are terrestrial higher plant biomarkers analysed in marine sedimentary archives to reconstruct continental palaeoclimatic and palaeohydrological conditions. Latitudinal variation in their concentration and distribution in marine sediments relatively close to the continent has been widely studied, but little is known on the extent to which this continental signal extends to the ocean. Furthermore, no studies have examined the seasonal variation in the deposition of these biomarkers in marine sediments. Here we studied longitudinal variation in the composition of long chain *n*-alkanes and two other terrestrial higher plant biomarkers (long chain *n*-alkanols and long chain fatty acids) in atmospheric particles, as well as longitudinal and seasonal variation in long chain *n*-alkanes in sinking particles in the ocean at different water depths and in surface sediments, all collected along a 12°N transect across the tropical North Atlantic Ocean. The highest abundance of all three biomarker classes was closest to the African coast, as expected, because they are transported with Saharan dust and the largest part of the dust is deposited close to the source. At this proximal location, the seasonal variability in long chain *n*-alkane flux and the chain length distribution of the *n*-alkanes in sinking particles was most pronounced, due to seasonal change in the dust source or to change in vegetation composition in the source area, related to the position of the Intertropical Convergence Zone (ITCZ). In contrast, in the open ocean the seasonal variability in both the long chain *n*-alkane flux and chain length distribution of the *n*-alkanes was low. The abundance of the alkanes was also lower, as expected because of the larger source-to-sink distance. At the western part of the transect, close to South America, we found an additional source of the alkanes in the sinking particles during spring and autumn in the year 2013. The $\delta^{13}C$ values of the alkanes in the surface sediment closest to the South American continent indicated that the isotope signal was likely derived from C_3 vegetation from the Amazon, implying an input from the Amazon River, as there is no significant aeolian input from South America there since the prevailing wind direction is from the east. Finally, the concentration of the alkanes was similar in the material collected from the atmosphere, the particles collected while settling through the marine water column, and in the surface sediments, providing evidence that degradation of long chain *n*-alkanes from the atmosphere to settling at the sediment–water interface at deep open ocean sites is minimal.

1. Introduction

The epicuticular wax of vascular plant leaves contains several series of long chain *n*-alkyl compounds, including *n*-alkanes, with typical chain length ranging from C_{25} to C_{35}, and *n*-alkanols and fatty acids (FAs) ranging from C_{16} to C_{36} (Eglinton and Hamilton, 1967). The long chain *n*-alkanes in particular are relatively resistant to degradation (Cranwell, 1981), making them useful as higher plant biomarkers in sediments. They typically have a strong odd/even predominance, while the long chain *n*-alkanols and FAs have a strong even/odd predominance (Eglinton and Hamilton, 1963). The predominance is expressed as the carbon preference index (CPI; Kolattukudy, 1976) and long chain *n*-alkanes from terrestrial

∗ Corresponding author at: NIOZ Royal Netherlands Institute for Sea Research, Department of Marine Microbiology and Biogeochemistry, and Utrecht University, P.O. Box 59, 1790 AB Den Burg, Texel, The Netherlands.
E-mail address: S.Schouten1@uu.nl (S. Schouten).

higher plants generally have CPI values > 5 (Eglinton and Hamilton, 1963; Diefendorf et al., 2011). Another parameter of interest is the chain length distribution, expressed as the average chain length (ACL), which depends on environmental conditions like aridity (Schefuß et al., 2003) or growth season temperature (e.g. Bendle et al., 2007), and on vegetation type (grasses vs. woody plants), although chain length distributions are variable within plant groups (Bush and McInerney, 2013). Therefore, interpretation of the ACL of long chain *n*-alkanes can be complicated. Finally, the stable carbon isotope composition of the alkanes can provide information on vegetation composition, as plants utilizing the C_3 photosynthetic pathway have *n*-alkane carbon isotope composition around −36‰ (−31‰ to −39‰), while plants utilizing the C_4 photosynthetic pathway have *n*-alkane carbon isotope composition around −21.5‰ (−18‰ to −25‰; e.g. Collister et al., 1994; Schefuß et al., 2003; Castañeda et al., 2009; Diefendorf and Freimuth, 2017).

Terrestrial higher plant biomarkers are transported to marine sediments in tropical oceans via water or wind, and can be carried to remote oceanic areas by aeolian transport (Gagosian and Peltzer, 1986). Consequently, they have been found in aeolian dust over the Atlantic Ocean close to the African continent (Simoneit, 1977), but also over more remote areas in the tropical North Pacific Ocean (Gagosian et al., 1981) and the South Pacific Ocean (Gagosian et al., 1987). Latitudinal variation in higher plant biomarkers in marine surface sediments proximal to the continent has been widely studied, both in the Atlantic Ocean (Huang et al., 2000; Schefuß et al., 2003, 2004) and the Pacific Ocean (Bendle et al., 2007; Horikawa et al., 2010), and have been shown to reflect latitudinal vegetation change on the continent. Thus, marine sediments form excellent archives of terrestrial biomarkers, which reflect continental-scale vegetation and climate change. However,

no study has examined the extent to which this continental signal carried by aeolian-transported terrestrial biomarkers extends to the ocean, i.e. the longitudinal source-to-sink variation in marine-deposited terrestrial biomarkers rather than the latitudinal variation. Furthermore, no studies have examined the seasonal variation in terrestrial biomarker deposition in the ocean as the above studies were carried out either on dust collected from the atmosphere, representing snapshots in time, or on surface sediments, representing an average of several decades to centuries of sediment deposition.

We focus here on a longitudinal transect at 12°N across the tropical North Atlantic Ocean (Fig. 1), where on average 182 Mt of dust from the Sahara are transported over the ocean every year, of which 140 Mt are deposited into the Atlantic (Yu et al., 2015). On the transect, marine sinking particles have been studied for seasonal and spatial variation in particle size of Saharan dust deposition (Van der Does et al., 2016), who found a downwind decrease in particle size and strong seasonal variability, with coarser dust in summer and finer dust in winter. Furthermore, Korte et al. (2017) studied mass flux values and composition and found the highest value close to the continents and a downwind change in mineralogical composition of Saharan dust, while Guerreiro et al. (2017) studied coccolithophore flux and found changes in species possibly related to Saharan dust. We report source-to-sink variation in the abundance and composition of long chain *n*-alkanes, long chain *n*-alkanols and FAs in Saharan dust collected between 2012 and 2015 along the same transect as the above studies, as well as seasonal and spatial variation in the input of long chain *n*-alkanes in sinking particles in the ocean at different water depths and in surface sediments along the 12°N transect. The results shed light on the source-to-sink distribution and depositional preservation of the continental long-chain *n*-alkane signal in the tropical North Atlantic Ocean.
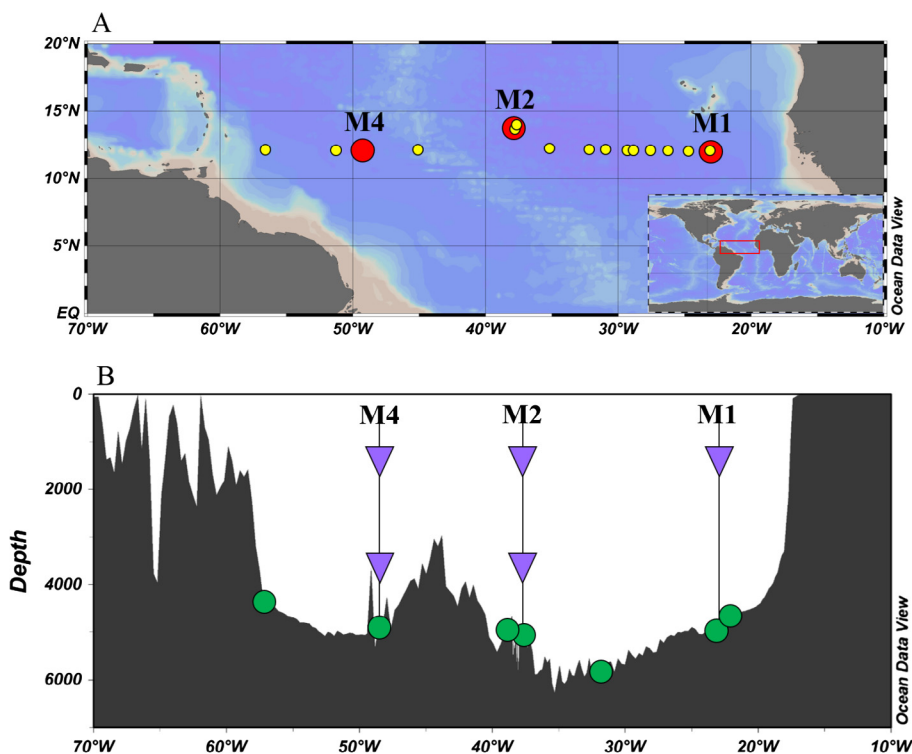
Fig. 1. (A) Longitudinal transect in tropical North Atlantic Ocean at 12°N with location of sites M1, M2 and M4 for sediment deployment (red circles) and location of dust sampling (yellow circles). The dust samples were taken either while sailing or while stationary, so the yellow circles represent either the middle of the sailed transect or the stationary location. In the bottom map (B) the location and depth of the traps (purple triangles) and surface sediments (green circles) is shown in a bathymetry map along the transect. Both maps were generated from Ocean Data View. (For interpretation of the references to color in this figure legend, the reader is referred to the web version of this article.)

2. Material and methods

2.1. Site description

The tropical North Atlantic Ocean receives Saharan dust input transported by three wind systems (Pye, 1987; Stuut et al., 2005; Muhs, 2013). First, dust is transported year-round in the shallow northeasterly trade wind layer, entraining dust from the Atlas Mountains, the coastal region of Morocco and parts of the northern Sahara. It is transported in a direction almost parallel to the coast, and is deposited in the proximal parts of the Atlantic Ocean, in a zone from the Canary Islands to the Cape Verde Islands. Second, the Harmattan trade winds transport dust from the central Sahara at an altitude between 0 and 3 km, again year-round, but more intensively during boreal winter, when the Intertropical Convergence Zone (ITCZ) migrates southward. Lastly, dust is transported with the Saharan Air Layer (SAL). In boreal summer, the ITCZ migrates north and moist tropical air from the south converges with dry hot Saharan air from the north and, with the convergence of these two air masses, dust is lifted to an altitude as high as 5–7 km. With this wind system, dust is transported from the Sahara and Sahel regions to more distal parts of the Atlantic Ocean. In the eastern tropical North Atlantic around 12°N, the influence of riverine input is limited as there are no major rivers discharging to this part of the ocean. However, in the western part, the Amazon river discharges on average 170 000 m^3s of water to the tropical Atlantic Ocean at the equator (Hellweger and Gordon, 2002), with seasonal variation in the direction of outflow. From February to May the flow is northwestward towards the Caribbean Sea and between June and January it is carried eastward towards Africa (Muller-Karger et al., 1988).

2.2. Sample collection

Samples were collected from the tropical North Atlantic along a transect at 12°N (Fig. 1). Surface sediments were taken on the M89 cruise with the R/V Meteor, between October 3 and 25, 2012 (Stuut et al., 2012), and on the 64PE378 cruise with the R/V Pelagia between November 9 and December 6, 2013 (Stuut et al., 2013). On the latter cruise, sediment trap samples were also retrieved. Atmospheric dust samples were collected during the 64PE395 cruise with the R/V Pelagia, between January 11 and February 6, 2015 (Stuut et al., 2015).

Air sampling was performed with an Anderson high volume dust collector (type HVP-5300AFC/230, "brushless automatic flow control outdoor Hi-Vol air sampler for continuous use"; purchased from Hi-Q, San Diego, USA) mounted on top of the bridge of the ship (for details see Stuut et al., 2015) along the 12°N transect (Fig. 1). The dust collector was connected to a wind vane programmed to have the unit switched on when wind was from a pre-determined arc of 100° to each side from the front of the ship, and off at other times to prevent contamination from the ship's chimney. The dust sampler was equipped with a motor which sucked ca. 70 m^3/h air through a glass fibre filter mounted on top; the filters were pre-combusted and stored in pre-combusted foil to prevent contamination of the samples. Sampling resulted in a total of 14 dust samples, which were collected for 10 h on average, with shortest collection time of 1.3 h and longest for 37.2 h, depending on the amount of dust in the air (Fig. 1; yellow circles). The 11 dust samples collected between M1 and M2 were obtained during one dust event, while the three samples further west were taken during another dust event. The samples were stored on board in a freezer at −80 °C until analysis in the laboratory. Sinking particulate matter (SPM) was collected with five sediment traps along the same transect at 12°N (Fig. 1), of which three were mounted on a cable

at 1200 m water depth, at mooring stations M1, M2 and M4 (Fig. 1) and two at 3500 m water depth, at mooring stations M2 and M4 (Fig. 1). All sediment traps were equipped with 24 sampling cups, collecting samples of SPM at intervals of 16 days from October 2012 until November 2013 (for details see Stuut et al., 2012, 2013; Van der Does et al., 2016; Korte et al., 2017). All 120 sediment trap samples were stored at 4 °C on board; back in the laboratory each sample was sieved through a 1 mm mesh to remove zooplankton swimmers and then wet-split into five aliquots using a WSD10 Rotor splitter (Van der Does et al., 2016). One of the aliquots was reserved for lipid analysis. In addition, surface sediments were collected with a multi-corer at 7 stations (Fig. 1; Stuut et al., 2012, 2013), of which the top 1 cm was sampled and stored at 4 °C until analysis.

2.3. Lipid analysis

2.3.1. Aeolian dust

All 14 glass fibre filters were cut into small (ca. 0.5 × 0.5 cm) pieces and ultrasonically extracted (5×) with dichloromethane (DCM):MeOH (2:1, v:v) and passed over a small Na_2SO_4 Pasteur pipette column. A known amount of squalane, hexadecan-2-ol and nonadecan-10-one was added to the extracts as internal standards for quantification. The extracts were methylated with BF_3/MeOH and separated into an apolar and a polar fraction on an activated Al_2O_3 column using hexane:DCM (1:1, v/v) and DCM:MeOH (1:1, v/v), respectively. The polar fraction contained the *n*-alkanols and the apolar fraction was further separated into an 'apolar' fraction, containing the *n*-alkanes, and a 'medium polarity' fraction, containing methylated FAs, by passing it over an Ag^+ impregnated silica column with hexane and DCM:MeOH (1:1, v/v), respectively. For *n*-alkanol analysis, the polar fraction was silylated using BSTFA [N,O-bis(trimethylsilyl)trifluoroacetamide] and pyridine, and heating at 60 °C for 20 min. Subsequently, the silylated fractions were dissolved in EtOAc, and those for *n*-alkane and FA analysis were dissolved in hexane. All samples were injected on-column with an Agilent 7890B gas chromatography (GC) instrument at 70 °C. The oven temperature was programmed to 130 °C at 20 °C/min, and subsequently to 320 °C (held 15 min) at 4 °C/min; He was the carrier gas at a constant 2 ml/min. Injection volume was 1 μl.

2.3.2. SPM and surface sediments

SPM and surface sediments were washed with Milli-Q water, freeze-dried and homogenized before extraction with DCM:MeOH (2:1, v:v) using ultrasonic extraction (5×), for which ca. 100 mg dry wt SPM and ca. 1.5–10 g dry wt surface sediment were used. Each extract was filtered over a small Na_2SO_4 Pasteur pipette column and a known amount of squalane was added as internal standard for quantification of the *n*-alkanes. The extract was separated into an apolar, a ketone and a polar fraction on an activated Al_2O_3 column with hexane:DCM (9:1, v:v), hexane:DCM (2:1, v:v) and DCM:MeOH (1:1, v:v), respectively, of which the apolar fraction was used to quantify the *n*-alkanes. For *n*-alkane analysis, the samples were dissolved in hexane and injected on-column on an Agilent 7890A GC instrument coupled to an Agilent 5975C mass spectrometry (MS) instrument. The GC conditions were as above, the only difference being that the oven temperature was held at 320 °C for 10 min instead of 15 min. The *n*-alkanes were quantified in full scan mode, scanning *m/z* 50–850.

2.4. Compound specific stable carbon isotope analysis

Long chain *n*-alkanes (C_{27} to C_{33}) in the surface sediments were analyzed for their stable carbon isotopic composition using GC–isotope ratio MS (GC–IRMS). The concentration in the dust and sediment-trap samples was too low for stable carbon isotopic

analysis. The *n*-alkanes were analyzed using a Thermo Delta V isotope IRM mass spectrometer coupled to an Agilent 6890 GC instrument. GC conditions were as for GC–MS. The samples were analyzed in duplicate and the reported data represent the mean stable carbon isotope value of duplicate runs. The values are reported in δ notation relative to the Vienna Peedee Belemnite (VPDB) using CO_2 reference gas calibrated to NBS-22 reference material. The instrument error was < 0.2‰ based on repeated injection of external deuteriated *n*-alkane standards (C_{20} and C_{24} perdeuteriated *n*-alkanes) prior to and after sample analysis. The weighted mean $\delta^{13}C$ of the long chain *n*-alkanes was calculated from the following:

$$\delta^{13}C_{27-33} = \sum(\delta^{13}C_{27} \times A_{27} + \delta^{13}C_{29} \times A_{29} + \delta^{13}C_{31} \times A_{31} + \delta^{13}C_{33} \times A_{33}) \Big/ \sum(A_{27} + A_{29} + A_{31} + A_{33}) \quad (1)$$

where $\delta^{13}C_{xx}$ is the isotope value of the long chain *n*-alkane and A the fractional abundance, normalized to the sum of the C_{27-33} abundances.

2.5. Higher plant biomarker based indices

ACL and CPI of the long chain *n*-alkanes, long chain *n*-alkanols and long chain FAs were calculated using the following:

$$ACL = \sum(I \times X_i) / \sum X_i \quad (2)$$

where X is abundance; i represents the carbon number of the *n*-alkane and ranges from 25 to 33 for long chain *n*-alkanes and from 28 to 32 for long chain *n*-alkanols and FAs.

The CPI of *n*-alkanes was calculated using the following:

$$CPI_{n\text{-alkanes}} = 1/2 \times \sum(X_{25} + X_{27} + X_{29} + X_{31} + X_{33}) \Big/ \sum(X_{24} + X_{26} + X_{28} + X_{30} + X_{32}) + 1/2 \times \sum(X_{25} + X_{27} + X_{29} + X_{31} + X_{33}) \Big/ \sum(X_{26} + X_{28} + X_{30} + X_{32} + X_{34}) \quad (3)$$

according to (Kolattukudy, 1976). A high value therefore indicates a high odd/even predominance.

The CPI of *n*-alkanol and FAs was calculated as follows:

$$CPI_{n\text{-alkanols and FAs}} = \sum(X_{28} + X_{30} + X_{32}) / \sum(X_{27} + X_{29} + X_{31}) \quad (4)$$

A high value indicates a strong even/odd predominance.

The fraction of short chain to long chain *n*-alkanes was calculated using the following:

$$\text{Short chain/long chain } n\text{-alkanes} = \sum(X_{16} + X_{17} + X_{18} + X_{19} + X_{20}) \Big/ \Big(\sum(X_{16} + X_{17} + X_{18} + X_{19} + X_{20}) + \sum(X_{25} + X_{27} + X_{29} + X_{31} + X_{33}) \Big) \quad (5)$$

For 2 out of 14 of the dust samples, the CPI of long chain *n*-alkanols could not be calculated as the odd carbon numbered *n*-alkanols were below detection limit. For 30 out of 120 of the sediment trap samples, the CPI of long chain *n*-alkanes could not be calculated due to the non-detection of even homologues.

3. Results

3.1. Aeolian dust

The concentration of dust in air varied between ca. 58 µg/m³ air close to the African continent and ca. 5 µg/m³ air in the samples

furthest away from Africa, and decreased with increasing distance from the coast (Fig. 2A). The concentration of long chain *n*-alkanes (C_{25}–C_{33}), long chain *n*-alkanols (C_{28}–C_{30}) and long chain FAs (C_{28}–C_{30}) in air also decreased with increasing distance from the African coast (Fig. 2A). The concentration of the *n*-alkanes varied between ca. 0.40 ng/m³ air close to the African continent and ca. 0.05 ng/m³ further away, while that of the *n*-alkanols varied between ca.1.20 and ca. 0.05 ng/m³ air and that of the FAs between ca. 0.22 and ca. 0.05 ng/m³ air (Fig. 2A). All dust samples showed a typical higher plant wax *n*-alkane, *n*-alkanol and FA distribution pattern with odd homologues dominating even homologues for the *n*-alkanes and even homologues dominating odd homologues for the *n*-alkanols and FAs. The odd/even predominance of the *n*-alkanes in dust, expressed as $CPI_{n\text{-alkanes}}$ (Eq. 3) was on average 2.4 ± 0.6, while the even/odd predominance values of the *n*-alkanols and FAs (as $CPI_{n\text{-alkanols}}$ and $CPI_{fatty\ acids}$, respectively; Eq. 4) were 9.5 ± 1.8 and 4.7 ± 1.4, respectively, and there was no clear downwind trend in CPI for any of the biomarkers (Fig. 2C). The ACL (Eq. 2) of the *n*-alkanes increased from ca. 27.2 close to the African coast to ca. 29.5 further away from the African continent (Fig. 2B). The trend was not visible in the *n*-alkanols or in the FAs; the ACL of these compounds was relatively stable over the transect, with an average of 29.4 ± 0.2 for the *n*-alkanols and 29.9 ± 0.1 for the FAs (Fig. 2B). Finally, to investigate sources of the long chain *n*-alkanes, the contribution of short chain *n*-alkanes (C_{16}, C_{17}, C_{18}, C_{19} and C_{20}) relative to the long chain *n*-alkanes (C_{25}, C_{27}, C_{29}, C_{31} and C_{33}) was calculated (Eq. 5; Fig. 2D). The values varied between 0.63 and 0.93, and did not show any particular trend with increasing longitude.

3.2. SPM

The total mass flux and the residual lithogenic mass flux of sinking particles collected at 1200 m water depth (Fig. 3B and C; from Korte et al., 2017) showed the highest flux at M1, closest to the African continent, the lowest at the open ocean location and a higher flux again at M4, closer to the South American continent. The same trend was visible for the long chain *n*-alkane flux. The highest flux was for the sediment trap at M1, with an average of 0.19 µg/m²/day (Fig. 3A). At this location, the flux was also the most variable of the three locations. In contrast, the sediment trap at the open ocean location (M2) yielded the lowest flux, with an average of 0.03 µg/m²/day, which was relatively more constant over the year (Fig. 3A). At M4, furthest from the African continent, the long chain *n*-alkane flux was slightly higher (avg. 0.07 µg/m²/day) than at the open ocean site, and was especially higher during two peaks in spring and fall (Fig. 3A). For the *n*-alkane flux and the total mass flux, there was no clear seasonal variability at any station (Fig. 3A and B), while the residual lithogenic flux showed a maximum in summer and fall at M1 (Fig. 3C; Korte et al., 2017). The flux weighted average ACL at M1 was 29.1, with slightly higher values in summer and lower values in winter (Fig. 3D). The same trend was visible at M4, although the flux weighted average ACL was slightly lower (28.7) than at M1. However, at M2 this trend was not present; instead, the ACL was stable throughout the year, with a flux weighted average value of 29.7. The CPI of the *n*-alkanes in the sinking particles was overall higher than in the aeolian dust from the atmosphere (avg. 2.4), with flux weighted average values of 5.0, 8.8 and 4.2 at M1, M2 and M4, respectively (Fig. 3E).

To investigate potential changes with respect to settling through the ocean, the flux, ACL and CPI values for the *n*-alkanes in sediment traps at two different water depths (1200 and 3500 m, hereafter called upper and lower trap, respectively) were compared, at M2 and M4 (Fig. 4). At M2, the average long chain
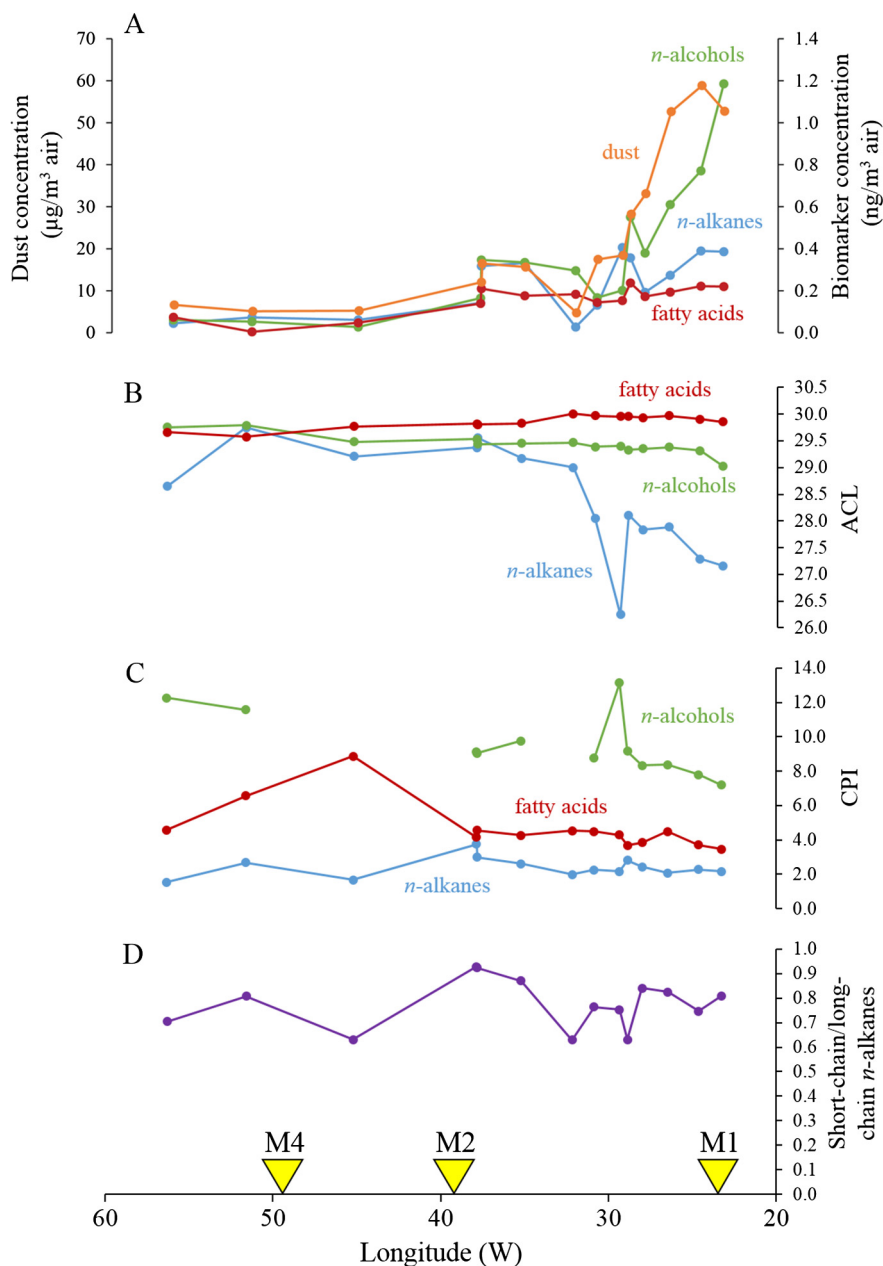
Fig. 2. (A) Concentration of dust (orange), long chain *n*-alkanes (C$_{25}$–C$_{33}$, blue), long chain *n*-alkanols (C$_{28}$–C$_{30}$, green) and long chain FAs (C$_{28}$–C$_{30}$, red), (B) ACL (Eq. 2), (C) CPI (Eqs. 3 and 4) and (D) fraction of short chain to long chain *n*-alkanes (Eq. 5), all plotted vs. degrees longitude (W). The yellow triangles in the bottom represent the locations of sediment traps on the transect. (For interpretation of the references to color in this figure legend, the reader is referred to the web version of this article.)

n-alkane flux in the lower sediment trap (Fig. 4A) was higher (0.05 µg/m²/day) than in the upper trap (0.03 µg/m²/day; Fig. 4A). The same trend was seen in the total mass flux and the residual lithogenic flux, which were on average also higher in the lower trap than in the upper trap (Fig. 4B and C). At M4, the opposite trend was observed (Fig. 4A), with a lower flux in the lower trap (avg. 0.04 µg/m²/day) vs. the upper sediment trap (avg. 0.07 µg/ m²/day). At this location, the total mass flux and the residual lithogenic flux were on average also lower in the lower trap than in the upper trap (Fig. 4B and C). For the ACL, at M2, the flux weighted average was lower (Fig. 4D) in the lower trap (29.2) than in the upper trap (29.7; Fig. 4D), while at M4 the flux weighted average ACL was higher in the lower trap (29.1) than in the upper trap (28.7). For the CPI (Fig. 4E), the flux weighted average at M2 was lower in the lower trap (4.0) than in the upper trap (8.8)

(Fig. 4E), and the opposite trend was observed at M4, with higher CPI in the lower trap (7.3) than in the upper trap (4.2).

3.3. Surface sediments

The long chain *n*-alkane concentration decreased from ca. 0.6 µg/g sediment, closest to the African continent, to ca. 0.1 µg/g further from Africa (Fig. 5A). The ACL and CPI values of the *n*-alkanes did not show any clear trend with increasing longitude and had average values of 29.9 ± 0.1 and 5.6 ± 1.5, respectively (Fig. 5B and C). The weighted mean δ¹³C of C$_{27}$-C$_{33}$ (Table 1) between 22 and 49°W was on average −25.5 ± 0.4‰ and did not show any clear trend with longitude (Fig. 5D). However, at the location closest to South America, the weighted mean δ¹³C value was more depleted at −27.1‰ (Table 1; Fig. 5D).
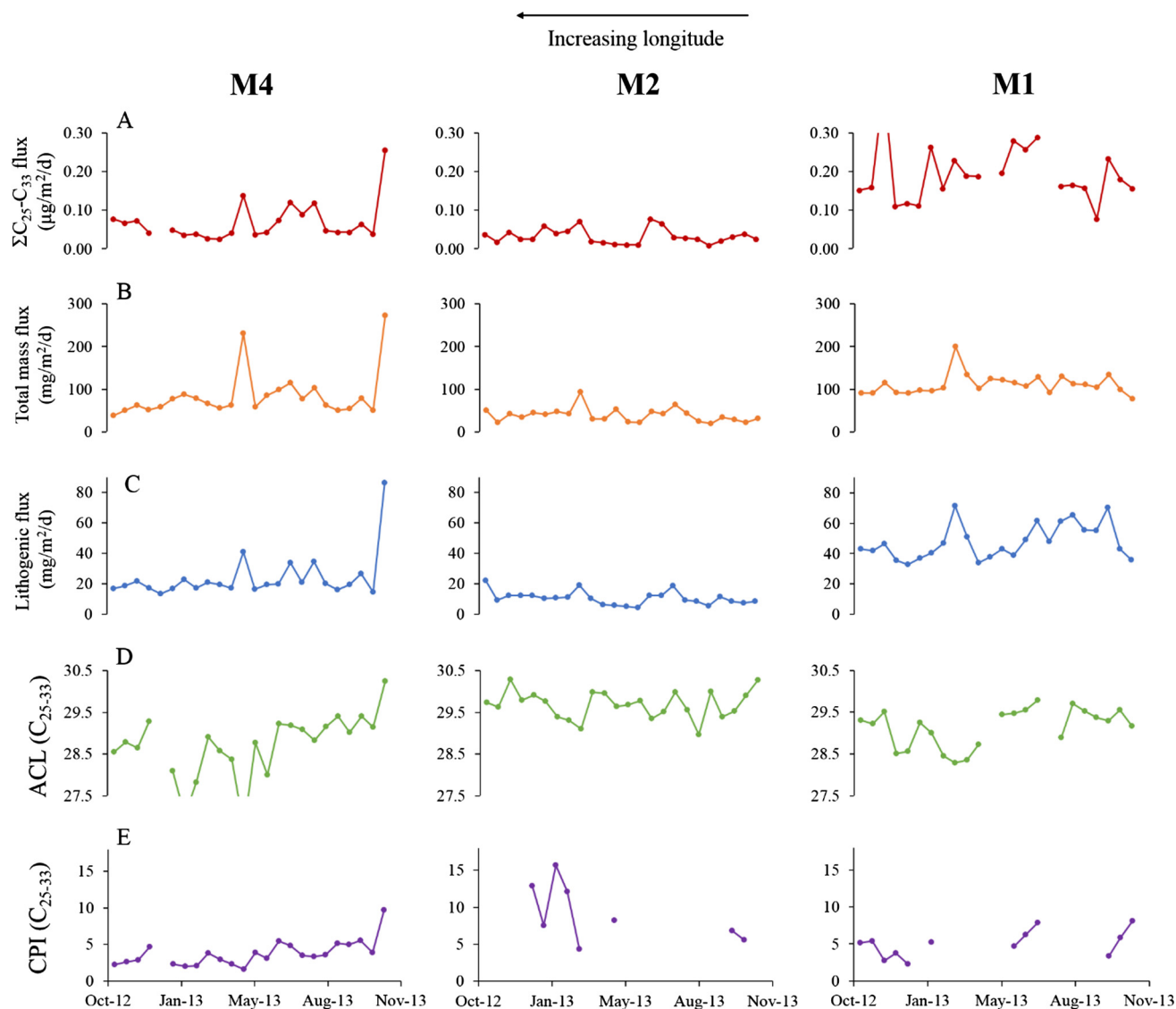
Fig. 3. Sediment trap time series from October 2012 to November 2013 at 1200 m water depth at M1, M2 and M4 of (A) long chain n-alkane flux (C_{25}–C_{33}), (B) total mass flux (from Korte et al., 2017), (C) residual lithogenic flux (from Korte et al., 2017), (D) ACL (C_{25-33}) (Eq. 2) and (E) CPI (C_{25-33}) (Eq. 3).

4. Discussion

4.1. Higher plant biomarkers in aeolian dust

Even though two different dust events were sampled, a decrease in concentration of long chain n-alkanes, n-alkanols and FAs in air with increasing distance from the African continent was observed (Fig. 2A), as expected, because close to the source, the largest part of the dust settles from the atmosphere due to gravitational settling (e.g. Schütz, 1980). Furthermore, the concentrations of n-alkanes, n-alkanols and FAs in the air (0.05–0.40, 0.05–1.20, 0.05–0.22 ng/m^3, respectively), are of the same order of magnitude as usually found in air at marine locations. For example, Simoneit (2006) reported a range of atmospheric concentrations of the n-alkanes, n-alkanols and FAs usually found over the ocean of 0.5–6, 0.1–5 and 0.1–21 ng/m^3, respectively. Furthermore, the concentrations here are also comparable with those at the western North Atlantic, at Bermuda, where the annual averages, measured over a 2.5 yr time series, were 0.45 ng/m^3 for the n-alkanes, 1.0 ng/m^3 for the n-alkanols and 1.2 ng/m^3 for the FAs (Conte and Weber, 2002).

The ACL of long chain n-alkanes in dust increases with longitude and is ca. 27–28 close to the African coast (Fig. 2B), lower than in dust taken off the coast of Africa around the same location (Huang et al., 2000; Eglinton et al., 2002; Schefuß et al., 2003), where ACL was reported to be close to 29. However, Huang et al. (2000) sampled dust in a different season (October–November 1970) and Eglinton et al. (2002) sampled dust over a longer time period (October 2012 to June 2013). This could possibly explain the differences, as seasonal change in the source of the dust or change in vegetation composition in the source area related to the position of the ITCZ would be expected. Schefuß et al. (2003) did sample dust in the same season (February–March 1998) as here, but found ACL values of long-chain n-alkanes of around 29. Higher values in dust are observed here further from the coast (Fig. 2B). In contrast to the n-alkanes, the ACL of the long chain n-alkanols and FAs is relatively stable and does not show an increasing trend with longitude (Fig. 2B). Furthermore, the CPI values for the n-alkanes (2.4 ± 0.6) are low compared with natural plant wax components, which typically have a high (> 5) CPI (Eglinton and Hamilton, 1963; Diefendorf et al., 2011), and are substantially lower than the n-alkanols (9.5 ± 1.8) and FAs (4.7 ± 1.4),
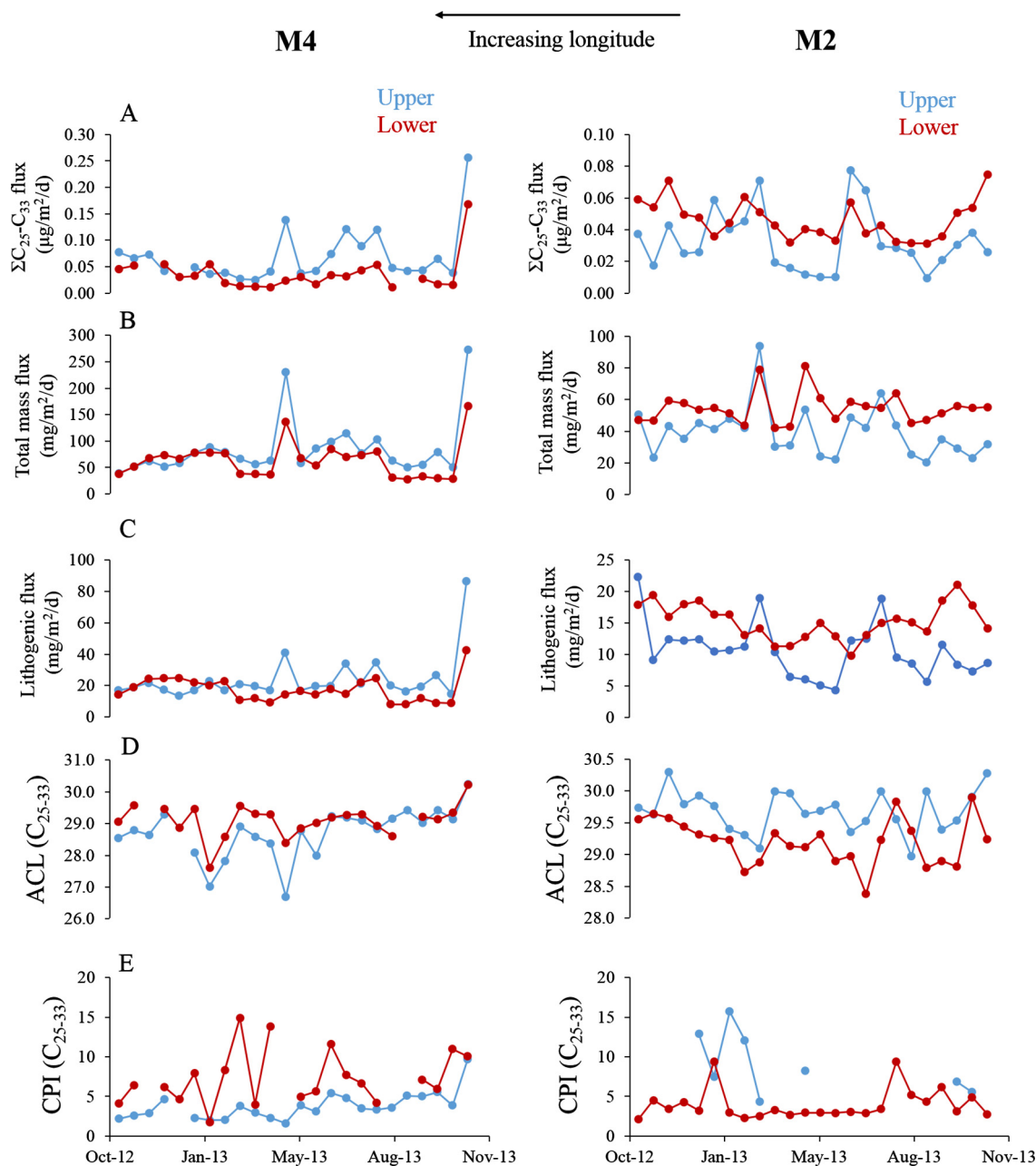
Fig. 4. Sediment trap time series from October 2012 to November 2013 at M2 and M4, at 1200 (blue) and 3500 m water depth (red) of (A) long chain n-alkane flux (C_{25}–C_{33}), (B) total mass flux (from Korte et al. (2017), (C) residual lithogenic flux (from Korte et al. (2017), (D) ACL ($C_{25–33}$) (Eq. 2) and (E) CPI ($C_{25–33}$) (Eq. 3). (For interpretation of the references to color in this figure legend, the reader is referred to the web version of this article.)

which have a strong even predominance (Fig. 2C). Collectively, this suggests an unusual input of n-alkanes with low CPI and ACL close to the African coast in our dust samples. These n-alkanes could come from a marine source, entering the atmosphere via sea spray (Lichtfouse et al., 1994), or from vehicle exhaust (Simoneit, 1984) either from the continent or from the ship, although contamination from the ship's funnel was kept to a minimum with the dust sampler programmed to only sample air when it came from the front of the ship. An input of vehicle exhaust would be expected to contain a high amount of short chain n-alkanes. However, the amount of short chain n-alkanes vs. that of long chain n-alkanes does not change with longitude (Fig. 2D), indicating that the input of short chain n-alkanes is constant and suggesting that the long chain n-alkanes with low CPI values are probably from sea spray.

4.2. Source-to-sink and seasonal change in n-alkane input to the tropical North Atlantic

The highest long chain n-alkane flux in the particles settling through the ocean was found at M1 (Fig. 3A), closest to the continent, and the highest concentration was found in the surface sediment (Fig. 5A). The concentration of long chain n-alkanes in the surface sediment at this location is 0.56 µg/g, comparable with the average concentration in surface sediments along the coast of Northwest Africa (0.7 ± 0.4 µg/g; Huang et al. (2000), 0.34–1.40 µg/g; Méjanelle and Laureillard (2008)). The CPI of long chain n-alkanes in the settling particles has a flux-weighted average of 5.0, comparable with that of long chain n-alkanes in the surface sediment at the same location (5.4; Fig. 5C). These values are
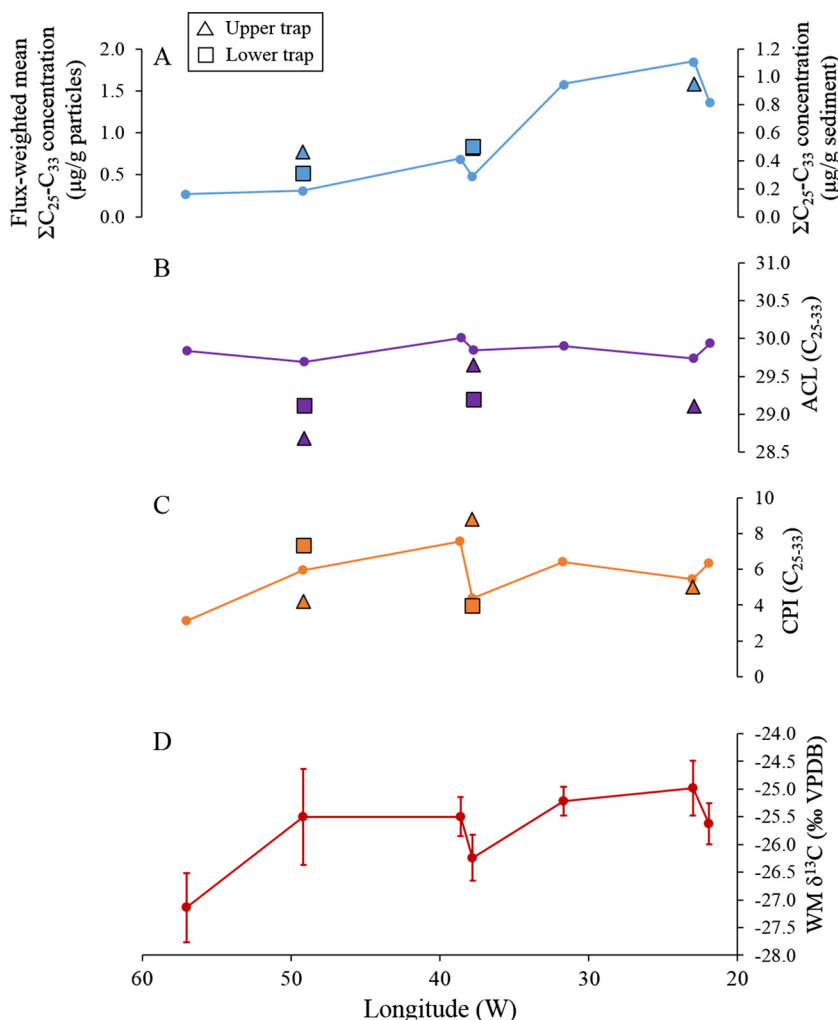
Fig. 5. (A) Concentration of long chain *n*-alkanes (C_{25}–C_{33}), (B) ACL (C_{25-33}) (Eq. 2), (C) CPI (C_{25-33}) (Eq. 3) and (D) weighted mean (WM) $\delta^{13}C$ value of long chain *n*-alkanes in surface sediments at 7 locations on the 12°N transect in the North Atlantic Ocean (for locations see Fig. 1B). The blue, purple and orange figures in A, B and C represent the flux-weighted average value for long chain *n*-alkane concentration, ACL and CPI, respectively, in sinking particles at M1, M2 and M4. The triangles represent the flux-weighted average values in the sinking particles at 1200 m water depth, while the squares represent flux-weighted average values from the sinking particles at 3500 m water depth. (For interpretation of the references to color in this figure legend, the reader is referred to the web version of this article.)

Table 1

The $\delta^{13}C$ values of long chain *n*-alkanes (C_{27}, C_{29}, C_{31} and C_{33}) and weighted mean $\delta^{13}C$ of long chain *n*-alkanes in 7 surface sediments on the 12°N transect in the North Atlantic Ocean.

Longitude (W)	$\delta^{13}C$ *n*-alkane				
	C_{27}	C_{29}	C_{31}	C_{33}	Weighted mean
21.9	−24.1	−26.9	−25.7	−24.7	−25.6
23.0	−23.8	−26.4	−24.9	−23.4	−25.0
31.7	−23.6	−26.6	−25.4	−24.0	−25.2
37.8	−24.7	−27.1	−26.1	−26.3	−26.2
38.6	−24.1	−26.5	−25.6	−24.5	−25.5
49.2	−23.9	−26.9	−25.4	−24.3	−25.5
57.0	−25.6	−28.2	−27.2	−26.3	−27.1

slightly higher than values for long chain *n*-alkanes in the same area (Huang et al., 2000; Méjanelle and Laureillard, 2008). The high values indicate that the long chain *n*-alkanes in the settling particles and surface sediments at M1 are derived predominantly from terrestrial higher plants. This also suggests that the unusually low CPI of *n*-alkanes in dust, as observed here is not representative for the longer term *n*-alkane signal as observed in the settling particles and the surface sediments. The weighted mean $\delta^{13}C$ of the long

chain *n*-alkanes in the surface sediment at M1, −25.0‰, is in agreement with an input of *n*-alkanes from mainly C_4 vegetation, as expected because the vegetation in the Sahara region is mainly C_4 (Collatz et al., 1998). The $\delta^{13}C$ value of the C_{29} long chain *n*-alkane is −26.4‰, slightly more positive than the value in surface sediments collected offshore Northwest Africa from 9–12°N latitude (−27‰ to −27.5‰; Huang et al. (2000); Castañeda et al. (2009)).

High long chain *n*-alkane flux and surface sediment concentration at M1 were expected because of the location close to the African continent (Fig. 1), where a large part of the dust particles settles out from the atmosphere (e.g. Schütz, 1980), as is also evident from the dust concentration in the air, with highest concentration close to the continent (Fig. 2A). The same trend is visible in the total mass flux (Fig. 3B) and the residual lithogenic flux (Fig. 3C), which are highest in the sediment trap at M1 (Korte et al., 2017). However, in the *n*-alkane flux and the total mass flux, there is no clear seasonal variability, while in the residual lithogenic flux there is a maximum in summer and fall at M1 (Fig. 3C). Due to the similarity in lithogenic particles collected in the sediment traps and dust collected at the African coast (Korte et al., 2017) and the absence of major rivers transporting sediment to the study area, it is assumed that the residual lithogenic flux

reflects dust transported from the Sahara, and is termed 'dust flux' below. The maximum dust flux in summer and fall is caused by the Saharan dust storms transported with the Saharan Air Layer (e.g. Stuut et al., 2005). However, there is no statistically significant correlation (Fig. 6) between the long chain n-alkane flux and the dust flux (R^2 0.035 and p = 0.406) in the sediment trap at M1, and also not between the long chain n-alkane flux and total mass flux (R^2 0.105 and p = 0.141). This is unexpected because long chain n-alkanes are thought to become airborne by being sloughed off the surface of leaves by wind, especially by a sandblasting effect (Simoneit, 1977) and transported with dust from the Sahara regions (Schefuß et al., 2003). This lack of coupling between the dust flux and the long chain n-alkane flux could be explained by the fact that in summer the ITCZ moves northward over the African continent, having a large effect on the origin of the aeolian dust and the pathways of the transported dust (Middleton and Goudie, 2001). During this period, dust is transported to the tropical North Atlantic with the SAL wind system, which picks up dust from the Bodélé depression in western Chad (Scheuvens et al., 2013). The vegetation in this region is relatively sparse, potentially resulting in less long chain n-alkanes transported during this period. In winter, the ITCZ moves southward, resulting in a change in the source of the dust to more coastal regions of Northwestern Africa, where different types of vegetation grow, possibly yielding a higher amount of long chain n-alkanes (Diefendorf and Freimuth, 2017). Alternatively, change in vegetation composition in the source area of the dust related to the position of the ITCZ rather than change in the geographical location of the dust source area could also explain the lack of coupling between the dust flux and the long chain n-alkane flux. Indeed, the concentration of long chain n-alkanes in the particles settling through the ocean is lower in summer than in winter, i.e. ca. 4 µg/g vs. ca. 2.5 µg/g. A seasonal change in the n-alkane source or in the vegetation composition in the source area is supported by the ACL, which shows slightly higher values in the summer period than in the winter period, indicating that the long chain n-alkanes are derived from a different vegetation type in summer than in winter. Long chain n-alkanes in sinking particles

at M1 thus seem to reflect change in source vegetation, which is supported by studies showing that plant wax components in dust primarily reflect vegetation type at the source region (e.g. Conte and Weber, 2002; Schefuß et al., 2003).

The lowest n-alkane flux, as well as total mass flux and dust flux (Fig. 3A–C) in the particles settling through the ocean was at M2, in the middle of the tropical North Atlantic Ocean. Also, the concentration in the surface sediment at this location is ca. 4× lower than at M1 (Fig. 5A). Interestingly, the n-alkane flux, total mass flux, dust flux and ACL were all relatively invariable over the year at this location (Fig. 3A–D). The low fluxes and seasonal variability in settling particles and low concentration in surface sediments of all particles are expected here because of the remote location away from the continents, where the continental signal is likely to be more smoothed out. Nonetheless, the weighted mean $\delta^{13}C$ value of the long chain n-alkanes in the surface sediments at M2 is similar to that at M1 (Fig. 5D), indicating that the n-alkanes deposited at both locations are likely from the same continental region (i.e. Africa). The flux-weighted average CPI of the particles settling through the ocean and in the surface sediments at M2 is comparable with values at M1, although the upper trap at M2 gives slightly higher values (Fig. 3E and 5C).

Interestingly, for the settling particles at M4, furthest from the African continent, the correlation between the n-alkane flux and dust flux (R^2 0.88 and p < 0.001) is strong, as well as the correlation between n-alkane flux and total mass flux (R^2 0.76 and p < 0.001; Fig. 6). The correlation between n-alkane flux and total mass flux indicates that at M4 the deposition of the n-alkanes is perhaps more strongly associated with deposition of marine biogenic particles in the ocean (e.g. Fischer and Karakaş, 2009) than at M1. The correlation between the n-alkane flux and dust flux, in contrast to the M1 site proximal to the African continent, suggests that the source of the n-alkanes is relatively constant over the year. The n-alkane ACL at this location shows more variability over the year than the other locations (Fig. 3D), while CPI is relatively stable with an average value comparable to that at M1. Also, the n-alkane flux is slightly higher at this location than at M2, with a peak in
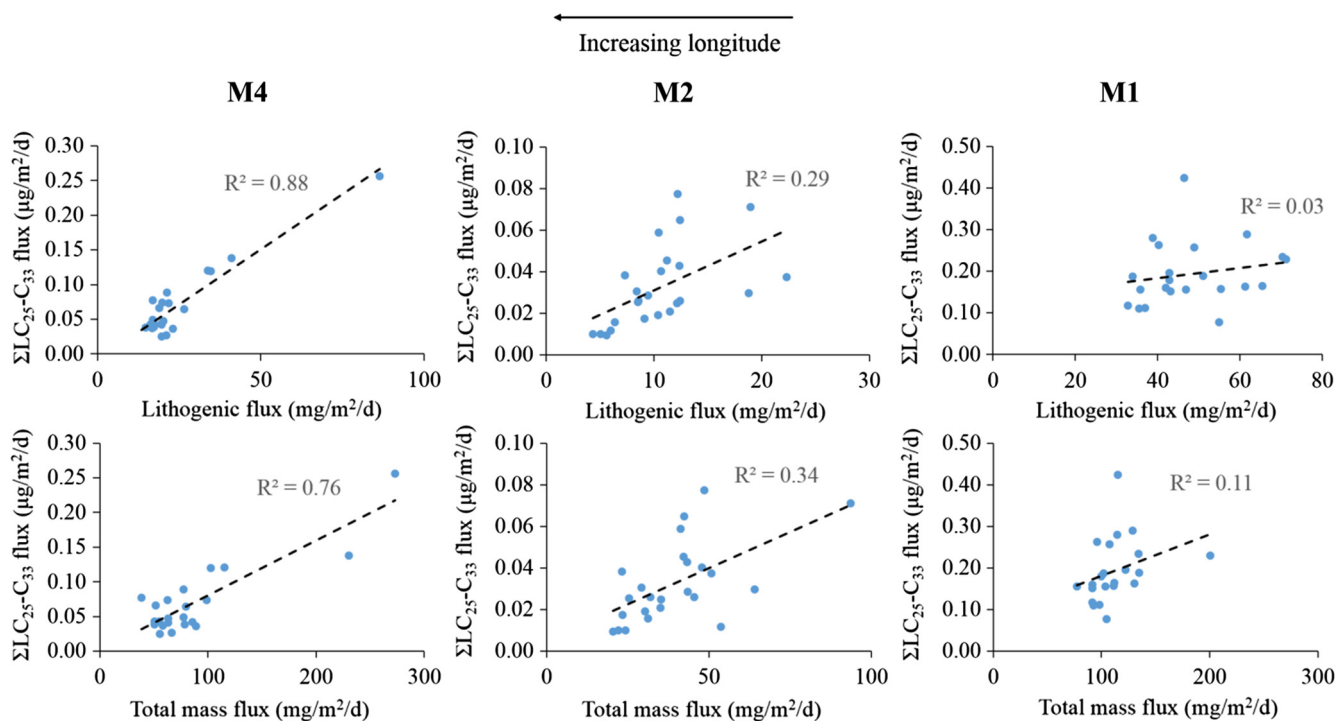
Fig. 6. Correlation of long chain n-alkane flux with residual lithogenic flux and total mass flux in sinking particles at 1200 m water depth at M1, M2 and M4.

April and October not seen at the other trap sites (Fig. 3A). This collectively indicates that at this location, there is an additional source of long chain *n*-alkanes in the settling particles besides that of Saharan dust. Indeed, Korte et al. (unpublished results) and (Guerreiro et al., 2017), showed that at M4 the total mass flux and the coccolithophore flux, respectively, are affected by the Amazon River in fall, when the Amazon discharge is carried offshore around a retroflection of the North Brazil Current and into the North Equatorial Counter Current. When retrieving the moorings in December 2013, Korte et al. (unpublished results) found that the Amazon River influence was present at M4, as indicated by low salinity and elevated silicate concentration in the surface mixed layer. Furthermore, Guerreiro et al. (2017) suggest that the peak in April is associated with enhanced export of organic material from the surface water down the water column due to nutrient enrichment of phytoplankton, acting as a ballast for sinking particles. Our results are in agreement with these findings, as we find the highest long chain *n*-alkane flux in April and October. However, we see neither a higher concentration of long chain *n*-alkanes in the surface sediments at M4 (Fig. 5A) compared with those more to the east, or different δ^{13}C values of the long chain *n*-alkanes at this location (Fig. 5D). This implies that the long chain *n*-alkanes transported by the Amazon River influenced the signal in the year that the sediment trap collected settling particles, but that it is not necessarily an influence every year. Interestingly, in the surface sediments further west of M4, closer to the South American coast, the weighted average δ^{13}C value of long chain *n*-alkanes is more depleted in ^{13}C (Fig. 5D), indicating an input from C$_3$ vegetation (e.g. Collister et al., 1994) such as from the Amazon rainforest. This implies that in the westernmost part of the transect, the influence of input from the Amazon River is more important and perennial than at location M4.

4.3. Preservation of n-alkane signal

The long chain *n*-alkane concentration in air at three locations close to M1, M2 and M4, sampled in January/February 2015, was compared with that in the sediment traps at 1200 m water depth, in the same months for the year 2013. The concentration in the air was 7.3, 15.5 and 14.4 µg/g dust at locations close to M1, M2 and M4, respectively, while the average concentration in the sediment trap in same period was 4.2, 3.1 and 2.8 µg/g dust (i.e. concentration normalized to the amount of residual lithogenic sediment) at M1, M2 and M4, respectively. Even though the *n*-alkane concentration in the air is a snapshot in time, the *n*-alkane concentration values in the atmosphere and in the ocean are quite similar, suggesting that the *n*-alkane signal is relatively well preserved from the air to the ocean at 1200 m water depth over the tropical North Atlantic Ocean.

To investigate the preservation of the *n*-alkane signal while settling through the water column, the *n*-alkane flux in the upper (1200 m) and lower (3500 m) sediment traps at M2 and M4 was compared. At M2, the *n*-alkane flux, total mass flux and dust flux are all higher in the lower trap compared with the upper trap (Fig. 4A–C). This could be explained by the bigger catchment area for the lower trap than the upper trap (Siegel and Deuser, 1997; Waniek et al., 2000) as also suggested by Korte et al. (2017), resulting in a higher input of particles in the lower trap. However, at M4 we did not see this enrichment of particles in the lower trap (Fig. 4A–C). Instead, the *n*-alkane flux is lower in the lower trap than the upper trap, and the same is apparent in the total mass flux and the dust flux. It could be that oceanic conditions, for example ocean currents, at this location are different from those at M2, leading to a different settling pathway of particles down the water column and, consequently, a different catchment area for the lower trap at M4. Regardless of this, there are no large and consistent dif-

ferences in the *n*-alkane flux between the lower and the upper sediment traps, which implies that degradation of long chain *n*-alkanes in the water column is not substantial.

To gain further insight into the preservation of the *n*-alkane signal during deposition, the flux-weighted average long chain *n*-alkane concentration, ACL and CPI in the particles settling through the ocean were compared with those of the surface sediments at the same locations (Fig. 5A–C). The long chain *n*-alkane concentration in the settling particles and that in the surface sediments show the same decreasing trend with distance to the African coast (Fig. 5A), and the concentration in the surface sediments is quite similar to that of the particles settling through the water column (Fig. 5A). This confirms that degradation of long-chain *n*-alkanes in surface sediments does not play a major role in the tropical North Atlantic Ocean. The CPI in the surface sediments also does not show any systematic difference with the CPI in the settling particles (Fig. 5C), indicating that in the surface sediments, the *n*-alkane signal is dominated by higher plant *n*-alkanes and that there is no substantial addition of marine even-numbered *n*-alkanes. Interestingly, the ACL of the *n*-alkanes in the surface sediments is consistently higher than the flux-weighted average ACL in the settling particles (Fig. 5B). This possibly indicates that the *n*-alkanes in the settling particles for the year in which they were collected had a slightly different source than those accumulating over the last decades to centuries in the surface sediments. This suggests that there is interannual variability in the composition of long chain *n*-alkanes exported to the tropical North Atlantic ocean floor, which is supported by the interannual variability observed in dust export to a sediment trap off Cape Blanc, Mauritania, between 1988 and 2012 (Fischer et al., 2016).

5. Conclusions

Long chain *n*-alkanes, derived from terrestrial higher plants, were detected in Saharan dust collected from the atmosphere, in particles settling through the ocean collected over one year and in surface sediments along a 12°N transect in the tropical North Atlantic Ocean. The highest abundance in the atmosphere, in the settling particles and in the surface sediments was closest to the African coast, where the largest part of the dust settles out of the atmosphere. At this proximal location, seasonal variability in the *n*-alkane flux and ACL of the *n*-alkanes in settling particles is pronounced, while in the open ocean, the long chain *n*-alkane flux in settling particles is lowest and seasonal variability in both the *n*-alkane flux and in the ACL is low. At the location closest to South America, there is an additional source of *n*-alkanes from the Amazon River in the settling particles. Indeed, further to the west, the δ^{13}C value of the *n*-alkanes in the surface sediment indicates an input of C$_3$ vegetation from the Amazon rainforest, implying that here the influence of input from the Amazon River is more important and perennial. Our results thus suggest that the aeolian transported *n*-alkanes from the African continent cross the entire equatorial Atlantic Ocean and can be recognized and quantified up to 4000 km from the African coast. Only at locations under the influence of the Amazon River is this signal diluted by an additional input of *n*-alkanes from the Amazon region. Furthermore, the study provides evidence that degradation of long chain *n*-alkanes from the atmosphere to settling at the sediment-water interface at deep open ocean sites is minimal.

Appendix A. Supplementary material

Supplementary data associated with this article can be found, in the online version, at https://doi.org/10.1016/j.orggeochem.2017.10.010.

*Associate Editor—***B. van Dongen**

References

Bendle, J., Kawamura, K., Yamazaki, K., Niwai, T., 2007. Latitudinal distribution of terrestrial lipid biomarkers and n-alkane compound-specific stable carbon isotope ratios in the atmosphere over the western Pacific and Southern Ocean. Geochimica et Cosmochimica Acta 71, 5934–5955.

Bush, R.T., McInerney, F.A., 2013. Leaf wax n-alkane distributions in and across modern plants: implications for paleoecology and chemotaxonomy. Geochimica et Cosmochimica Acta 117, 161–179.

Castañeda, I.S., Mulitza, S., Schefuß, E., Lopes dos Santos, R.A., Sinninghe Damsté, J.S., Schouten, S., 2009. Wet phases in the Sahara/Sahel region and human migration patterns in North Africa. Proceedings of the National Academy of Sciences 106, 20159–20163.

Collatz, G.J., Berry, J.A., Clark, J.S., 1998. Effects of climate and atmospheric CO_2 partial pressure on the global distribution of C_4 grasses: present, past, and future. Oecologia 114, 441–454.

Collister, J.W., Rieley, G., Stern, B., Eglinton, G., Fry, B., 1994. Compound-specific $\delta^{13}C$ analyses of leaf lipids from plants with differing carbon dioxide metabolisms. Organic Geochemistry 21, 619–627.

Conte, M.H., Weber, J., 2002. Long-range atmospheric transport of terrestrial biomarkers to the western North Atlantic. Global Biogeochemical Cycles 16.

Cranwell, P., 1981. Diagenesis of free and bound lipids in terrestrial detritus deposited in a lacustrine sediment. Organic Geochemistry 3, 79–89.

Diefendorf, A.F., Freeman, K.H., Wing, S.L., Graham, H.V., 2011. Production of n-alkyl lipids in living plants and implications for the geologic past. Geochimica et Cosmochimica Acta 75, 7472–7485.

Diefendorf, A.F., Freimuth, E.J., 2017. Extracting the most from terrestrial plant-derived n-alkyl lipids and their carbon isotopes from the sedimentary record: a review. Organic Geochemistry 103, 1–21.

Eglinton, G., Hamilton, R., 1963. The distribution of alkanes. Chemical Plant Taxonomy 187, 217.

Eglinton, G., Hamilton, R.J., 1967. Leaf epicuticular waxes. Science 156, 1322–1335.

Eglinton, T., Eglinton, G., Dupont, L., Sholkovitz, E., Montluçon, D., Reddy, C., 2002. Composition, age, and provenance of organic matter in NW African dust over the Atlantic Ocean. Geochemistry, Geophysics, Geosystems 3, 1–27.

Fischer, G., Karakaş, G., 2009. Sinking rates and ballast composition of particles in the Atlantic Ocean: implications for the organic carbon fluxes to the deep ocean. Biogeosciences 6, 85–102.

Fischer, G., Romero, O., Merkel, U., Donner, B., Iversen, M., Nowald, N., Ratmeyer, V., Ruhland, G., Klann, M., Wefer, G., 2016. Deep ocean mass fluxes in the coastal upwelling off Mauritania from 1988 to 2012: variability on seasonal to decadal timescales. Biogeosciences 13, 3071–3090.

Gagosian, R.B., Peltzer, E.T., 1986. The importance of atmospheric input of terrestrial organic material to deep sea sediments. Organic Geochemistry 10, 661–669.

Gagosian, R.B., Peltzer, E.T., Merrill, J.T., 1987. Long-range transport of terrestrially derived lipids in aerosols from the South Pacific. Nature 325, 800–803.

Gagosian, R.B., Peltzer, E.T., Zafiriou, O.C., 1981. Atmospheric transport of continentally derived lipids to the tropical North Pacific. Nature 291, 312–314.

Guerreiro, C.V., Baumann, K.-H., Brummer, G.-J.A., Fischer, G., Korte, L.F., Merkel, U., Sa, C., De Stigter, H., Stuut, J.B.W., 2017. Coccolithophore fluxes in the open tropical North Atlantic: influence of the Amazon river and of Saharan dust deposition. Biogeosciences 14, 1–22.

Hellweger, F.L., Gordon, A.L., 2002. Tracing Amazon river water into the Caribbean Sea. Journal of Marine Research 60, 537–549.

Horikawa, K., Murayama, M., Minagawa, M., Kato, Y., Sagawa, T., 2010. Latitudinal and downcore (0–750 ka) changes in n-alkane chain lengths in the eastern equatorial Pacific. Quaternary Research 73, 573–582.

Huang, Y., Dupont, L., Sarnthein, M., Hayes, J.M., Eglinton, G., 2000. Mapping of C_4 plant input from North West Africa into North East Atlantic sediments. Geochimica et Cosmochimica Acta 64, 3505–3513.

Kolattukudy, P.E., 1976. Chemistry and Biochemistry of Natural Waxes. Elsevier Scientific Pub. Co..

Korte, L.F., Brummer, G.-J.A., Van der Does, M., Guerreiro, C.V., Hennekam, R., Hateren, J.A.v., Jong, D., Munday, C.I., Schouten, S., Stuut, J.-B.W., 2017. Downward particle fluxes of biogenic matter and Saharan dust across the equatorial North Atlantic. Atmospheric Chemistry and Physics 17, 6023–6040.

Lichtfouse, E., Derenne, S., Mariotti, A., Largeau, C., 1994. Possible algal origin of long chain odd n-alkanes in immature sediments as revealed by distributions and carbon isotope ratios. Organic Geochemistry 22, 1023–1027.

Méjanelle, L., Laureillard, J., 2008. Lipid biomarker record in surface sediments at three sites of contrasting productivity in the tropical North Eastern Atlantic. Marine Chemistry 108, 59–76.

Middleton, N., Goudie, A., 2001. Saharan dust: sources and trajectories. Transactions of the Institute of British Geographers 26, 165–181.

Muhs, D.R., 2013. The geologic records of dust in the Quaternary. Aeolian Research 9, 3–48.

Muller-Karger, F.E., McClain, C.R., Richardson, P.L., 1988. The dispersal of the Amazon's water. Nature 333, 56–59.

Pye, K., 1987. Aeolian Dust and Dust Deposits. Academic Press, London, p. 334.

Schefuß, E., Ratmeyer, V., Stuut, J.-B.W., Jansen, J.S., Sinninghe Damsté, J.S., 2003. Carbon isotope analyses of n-alkanes in dust from the lower atmosphere over the central eastern Atlantic. Geochimica et Cosmochimica Acta 67, 1757–1767.

Schefuß, E., Versteegh, G.J., Jansen, J., Sinninghe Damsté, J., 2004. Lipid biomarkers as major source and preservation indicators in SE Atlantic surface sediments. Deep Sea Research Part I: Oceanographic Research Papers 51, 1199–1228.

Scheuvens, D., Schütz, L., Kandler, K., Ebert, M., Weinbruch, S., 2013. Bulk composition of northern African dust and its source sediments—a compilation. Earth Science Reviews 116, 170–194.

Schütz, L., 1980. Long range transport of desert dust with special emphasis on the Sahara. Annals of the New York Academy of Sciences 338, 515–532.

Siegel, D., Deuser, W., 1997. Trajectories of sinking particles in the Sargasso Sea: modeling of statistical funnels above deep-ocean sediment traps. Deep Sea Research Part I: Oceanographic Research Papers 44, 1519–1541.

Simoneit, B.R., 1977. Organic matter in aeolian dusts over the Atlantic Ocean. Marine Chemistry 5, 443–464.

Simoneit, B.R., 1984. Organic matter of the troposphere—III, 1967. Characterization and sources of petroleum and pyrogenic residues in aerosols over the western United States. Atmospheric Environment 18, 51–67.

Simoneit, B.R., 2006. Atmospheric transport of terrestrial organic matter to the sea. In: Volkman, J.K. (Ed.), Marine Organic Matter: Biomarkers. Springer, Isotopes and DNA, pp. 165–208.

Stuut, J.B., Boersen, B., Bruck, H.M., Hansen, A., Koster, B., Van der Does, M., Witte, Y., 2012. Cruise Report RV Meteor M89, TRAFFIC I: Transatlantic Fluxes of Saharan Dust, 3–25 October 2012.

Stuut, J.B., Brummer, G.J.A., Van der Does, M., Friese, C., Geerken, E., van der Heide, R., Korte, L., Koster, B., Metcalfe, B., Munday, C.I., van Ooijen, J., Siccha, M., Veldhuizen, R., de Visser, J.-D., Witte, Y., Wuis, L., 2013. Cruise Report RV Pelagia 64PE378, TRAFFIC II: Transatlantic Fluxes of Saharan Dust, 9 November–6 December 2013.

Stuut, J.B., Witte, Y., de Visser, J.-D., Boersen, B., Koster, B., Bakker, K., Laan, P., Van der Does, M., Korte, L., Munday, C., van Hateren, H., 2015. Cruise Report RV Pelagia 64PE395, TRAFFIC III: Transatlantic Fluxes of Saharan Dust, 11 January–6 February 2015.

Stuut, J.B., Zabel, M., Ratmeyer, V., Helmke, P., Schefuß, E., Lavik, G., Schneider, R., 2005. Provenance of present-day aeolian dust collected off NW Africa. Journal of Geophysical Research: Atmospheres 110.

Van der Does, M., Korte, L.F., Munday, C.I., Brummer, G.-J.A., Stuut, J.-B.W., 2016. Particle size traces modern Saharan dust transport and deposition across the equatorial North Atlantic. Atmospheric Chemistry and Physics 16, 13697–13710.

Waniek, J., Koeve, W., Prien, R.D., 2000. Trajectories of sinking particles and the catchment areas above sediment traps in the northeast Atlantic. Journal of Marine Research 58, 983–1006.

Yu, H., Chin, M., Bian, H., Yuan, T., Prospero, J.M., Omar, A.H., Remer, L.A., Winker, D. M., Yang, Y., Zhang, Y., 2015. Quantification of trans-Atlantic dust transport from seven-year (2007–2013) record of CALIPSO lidar measurements. Remote Sensing of Environment 159, 232–249.